Drug Designing: Open Access
ISSN: 2169-0138

Sun et al., Drug Des 2017, 6:1
DOI: 10.4172/2169-0138.1000142

Research Article Open Access

An Integrated Computational and Experimental Binding Study Identifies the DNA Binding Domain as the Putative Binding Site of Novel Pyrimidinetrione Signal Transducer and Activator of Transcription 3 (STAT3) Inhibitors

Shan Sun[1,3], Peibin Yue[2], Mingzhu He[3], Xiaolei Zhang[2], David Paladino[2], Yousef Al-Abed[3], James Turkson[2]* and John K Buolamwini[1,4]*

[1]Department of Pharmaceutical Sciences, College of Pharmacy, University of Tennessee Health Science Center, 847 Monroe Avenue, Suite 327, Memphis, TN 38163, USA
[2]University of Hawaii Cancer Center, Cancer Biology and Natural Products and Experimental Therapeutic Programs, 701 Ilalo Street, Suite 344, Honolulu, HI 96813, USA
[3]Center for Molecular Innovation, The Feinstein Institute for Medical Research, 350 Community Drive, Manhasset, NY11030, USA
[4]Department of Pharmaceutical Sciences, College of Pharmacy, Rosalind Franklin University of Medicine and Science, 3333 Green Bay Road, North Chicago, IL 60064, USA

Abstract

Objective: Signal transducer and activator of transcription 3 (STAT3) is as a potential drug target for cancer and inflammation. Strategies to block STAT3 dimerization have dominated STAT3 inhibitor discovery, while inhibition of direct STAT3-DNA binding has not been much explored. This study was to identify novel STAT3 inhibitors that may be developed into probes or therapeutics, and to investigate their putative binding site.

Methods: A library of in-house compounds was screened against STAT3-DNA binding using an electrophoretic mobility shift assay (EMSA). Inhibition of DNA and STAT3:STAT3 or STAT3:STAT1 interaction and antiproliferative activity in STAT3 expressing or STAT3 knockout cells were tested. Pharmacophore modeling and 3D-QSAR; and docking with molecular mechanics generalized born surface area (MM-GBSA) refinement were also undertaken at the STAT3 SH2 and STAT3 DNA binding domains. Surface plasmon resonance (SPR) analysis was done to determine STAT3 domain interactions. Organic synthesis was also undertaken.

Results: Pyrimidinetriones derivatives were identified as novel STAT3 inhibitors, with activity in low micromolar concentrations. Application of 3D-QSAR and docking analysis with MM-GBSA refinement suggested that the compounds bind at the STAT3-DNA binding interface, and not at the SH2 domain where most current STAT3 inhibitors are thought to bind. The results were confirmed with SPR analysis, pointing to the DNA binding domain (DBD) as the putative binding site of this novel class of STAT3 inhibitors. The analysis guided the synthesis of active novel compounds.

Conclusion: Pyrimidinetrione were identified as new STAT3 inhibitors that putatively bind at the STAT3 DBD. This study is an excellent example of the use of QSAR and structure-based design to aid the identification of putative ligand binding sites on proteins. The compounds will provide new tools for studying STAT3 biology; and also serve as potential leads for the development of new therapeutics against STAT3 to fight or study diseases such as cancer and inflammation.

Keywords: Docking; MM-GBSA; Pharmacophore-based 3D-QSAR; STAT3 DNA binding site; STAT3 inhibitors; Electrophoretic mobility assay; Surface plasmon resonance assay

Introduction

Signal transducers and activators of transcription (STATs) regulate gene expression in normal cellular responses to cytokines and growth factors [1-3]. STAT3 is the most studied one of the 7 family members identified due to its major mediatory effects on carcinogenesis and inflammation [2,4]. The aberrant activation of STAT3 has been detected in a wide variety of human cancer cell lines and tissues [5].

Constitutively active STAT3 suppresses apoptosis [6], upregulates the expression of cell proliferation genes [7,8], stimulates tumor angiogenesis [9] and opposes anti-tumor immune responses [10,11]. Hence, STAT3 is considered as a promising therapeutic target for cancer therapy.

STAT3 activation begins with the phosphorylation of a critical tyrosine residue (Tyr705) on its Src homology 2 (SH2) domain by activated growth factor receptors, Janus kinases (JAKs) or Src tyrosine kinase. Upon activation, STAT3 forms dimers through a reciprocal phosphotyrosine (pTyr705):SH2 domain interaction and translocates to the nucleus where the dimers bind to the promoters of target genes and activate specific gene expression. For many years, the SH2 domain-pTyr dimerization step was regarded as an attractive target for interfering with STAT3 function and this strategy has been exploited in many STAT3 drug discovery approaches [12]. Most nonpeptide STAT3 inhibitors known to date are small molecule compounds and

***Corresponding authors:** John K Buolamwini, Department of Pharmaceutical Sciences, College of Pharmacy, Rosalind Franklin University of Medicine and Science, 3333 Green Bay Road, North Chicago, IL 60064, United States, Tel: 847-578-8341; E-mail: john.buolamwini@rosalindfranklin.edu

James K Turkson, University of Hawaii Cancer Center, Cancer Biology and Natural Products and Experimental Therapeutic Programs, 701 Ilalo Street, Suite 344, Honolulu, HI 96813, United States, Tel: 808-356-5784; E-mail: jturkson@mail.ucf.edu

Received January 11, 2017; **Accepted** January 31, 2017; **Published** February 07, 2017

Citation: Sun S, Yue P, He M, Zhang X, Paladino D, et al. (2017) An Integrated Computational and Experimental Binding Study Identifies the DNA Binding Domain as the Putative Binding Site of Novel Pyrimidinetrione Signal Transducer and Activator of Transcription 3 (STAT3) Inhibitors. Drug Des 6: 142. doi: 10.4172/2169-0138.1000142

peptidomimetics, such as Stattic [13], STA-21 [14], S31-201 [15], LLL-12 [16], 14aa [17], etc., and are mainly STAT3 dimerization disrupting agents. Unfortunately, none of these STAT3 dimerization disrupting agents has reached the clinic as cancer therapeutics. In contrast to STAT3 dimerization disrupting agents, not much progress has been made in approaches aimed at direct inhibition of STAT3 DNA binding [18,19]. Recent studies have indicated that STAT3 nuclear import can take place constitutively and independently of Tyr705 phosphorylation through the nuclear import carrier importin-α3 [20]. In addition, the binding of unphosphorylated STAT3 directly to DNA has also been observed by an electrophoretic mobility shift assay (EMSA) [21]. These studies suggest that the strategy of blocking STAT3 dimerization by targeting the SH2 domain might be unable to effectively inhibit STAT3 activity. Although a number of molecules have been screened or developed as putative STAT3 SH2 domain binding inhibitors, binding sites for these small molecules at the SH2 domain have not been identified by any crystal structure.

In early 2000, a tetrahyroisobenzofuranone derivative [22] and a class of platinum (IV) compounds [23,24] were reported to potentially interact with the STAT3 DNA binding domain (DBD) and in turn inhibited STAT3-DNA binding and transcriptional activities; but the exact mode of inhibition of STAT3 is not understood. A peptide aptamer has also been identified as a STAT3 inhibitor that specifically interacts with the STAT3 DBD [25,26]. Recently, selective STAT3 DBD inhibitors with the 5-phenyl-1H-pyrrolo-2(3H)-ketone core structure were reported to directly bind to the DBD and inhibit the DNA binding activity of STAT3 both *in vitro* and *in situ* [19,27]. The reason for the low interest in STAT3:DNA-binding interface could be the notion that DBDs of transcription factors are generally "undruggable", often being flat and of limited selectivity [28,29]. The inability of any of the many small molecule STAT3 SH2 domain to progress to the clinic so far, gives cause to pursue other STAT3 domain binding inhibitors such as the DBD inhibitors.

We carried out an unbiased screening of in-house compound libraries using electrophoretic mobility shift assay (EMSA) to identify novel inhibitors preventing STAT3-DNA binding. The hits indicated that the pyrimidinetrione system constituted a novel STAT3 inhibitor scaffold. We further pursued it by testing additional pyrimidinetrione derivatives and developed a structure-activity relationship (SAR). We then set about to using computational docking and pharmacophore mapping and 3D-QSAR modeling to investigate which of the two major STAT3 domains, i.e., SH2 and DBD, this novel class of inhibitors bind to. With this approach, we expanded the SAR and conducted pharmacophore mapping and 3D-QSAR studies using both a *cis*-conformational alignment and a trans-conformational alignment. In parallel, we applied structure-based modeling studies, including binding site mapping, docking and the molecular mechanics generalized born surface area (MM-GBSA)-based refinement analysis, to explore the binding pocket and poses of this class of compounds. Finally, surface plasmon resonance (SPR) studies were used to interrogate the suggestion by the computational studies that the novel pyrimidinetrione STAT3 inhibitors bind to the DBD STAT3, but not the SH2 domain.

Results

In vitro screening for selective STAT3 inhibitor lead structures

To develop novel drug leads, more than 300 in-house compounds were screened for their inhibitory effects on STAT3-DNA binding by electrophoretic mobility shift assay (EMSA) *in vitro* at 10 μM. Two hits, **1** and **2**, which shared a common pyrimidinetrione core structure were evaluated in STAT3-DNA binding assay as previously reported [23,24]. Nuclear extracts containing active STAT3 prepared from v-Src-transformed mouse fibroblasts (NIH3T3/v-Src) were incubated for 30 min at room temperature with or without increasing concentrations of the hits, prior to incubation for 30 min with the radiolabeled hSIE probe, which binds to STAT3 and STAT1 and subjected to EMSA analysis [23,24]. Both compound **1** and **2** exhibited a dose-dependent inhibition of STAT3-DNA binding activity with IC_{50} values of 2.5 μM and 3.80 μM, respectively (Figure 1A). These values represent a dramatic improvement over those reported STAT3 inhibitors [18]. For selectivity, nuclear extracts containing active STAT1 and STAT3 prepared from the epidermal growth factor (EGF)-stimulated mouse fibroblasts over-

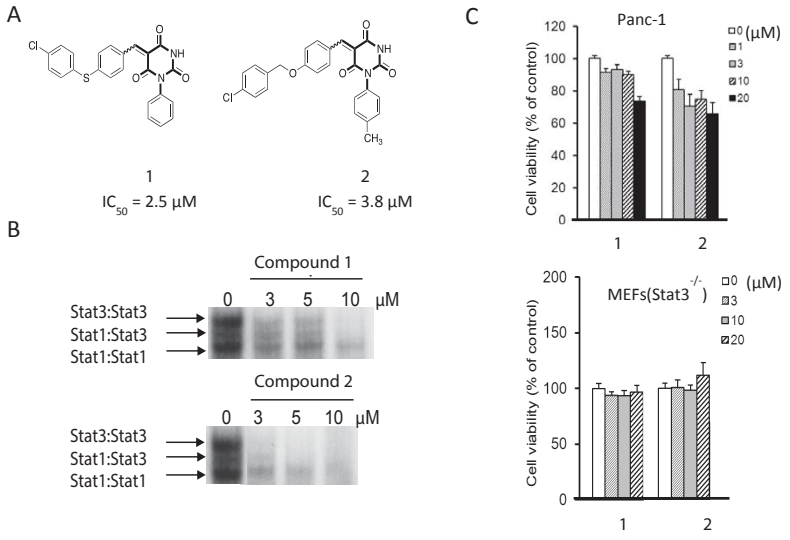

Figure 1: Selective effects of compounds **1** and **2** on the activities of STAT3. (A) Structure of compounds 1 and 2. Pyrimidinetrione lead structure is highlighted. (B) Nuclear extracts of equal total protein containing activated STAT1 and/or STAT3 were pre-incubated with or without compounds 1 or 2 for 30 min at room temperature prior to the incubation with the radiolabeled hSIE probe that binds Stat1 and Stat3, and subjected to EMSA analysis. (C) Effects of compounds 1 and 2 on pancreatic cancer cells (Panc-1) that harbor constitutively-active STAT3 and STAT3 knockout mouse embryonic fibroblasts (MEFs/STAT3-/-).

No.	X	R_1	R_2	Activity	
				IC_{50} (μM)	pIC_{50}[a]
*1	O	Ph	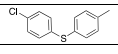	2.50	5.602
2	O	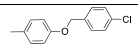	4-methyl-Ph	3.80	5.420
3	O	CH_3	4-methoxy-Ph	68.60	4.164
4	O	Ph	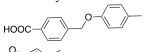	8.50	5.071
5	O	1-naphthaiene		5.24	5.281
6	O	3-methyl-Ph	2,4-dimethoxy-Ph	13.30	4.876
7	O	4-methyl-Ph		4.70	5.328
*8	O	4-methoxy-Ph	2-furan	408.00	3.389
9	O	4-methoxy-Ph	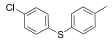	3.28	5.484
10	O	2-F-Ph	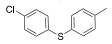	2.13	5.672
11	O	4-F-Ph		16.23	4.790
*12	O	4-F-Ph	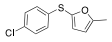	7.46	5.127
13	S	3-Cl-Ph		4.51	5.346

No.	X	R_1	R_2	Activity	
				IC_{50} (μM)	pIC_{50}[a]
14	O	4-Cl-Ph		128.40	3.891
15	O	4-Cl-Ph	5-methyl-2-furan	500.00	3.301
*16	S	4-Br-Ph		59.75	4.224
17	O	4-Br-Ph		4.71	5.327
*18	O			5.07	5.295
19	O	4-OH-Ph	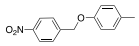	10.00	5.000
20	O	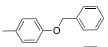	3-methoxy-Ph	11.50	4.939
21	O	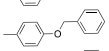	Ph	10.34	4.985
22	O	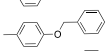	4-OH-Ph	31.70	4.499
*23	O	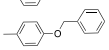	3-OH-Ph	11.60	4.936
24	O	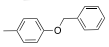		37.30	4.428
25	O	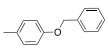		8.14	5.089
26	O	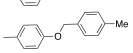	4-methoxy-Ph	16.40	4.785

No.	X	R_1	R_2	Activity	
				IC_{50} (μM)	pIC_{50}[a]
27	O	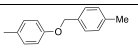	3,4-dimethoxy-Ph	8.56	5.068
28	O	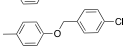		7.41	5.130
29	O	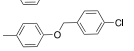	4-methoxy-Ph	8.02	5.096
30	O	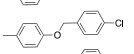	3-Cl-4-Me-Ph	17.77	4.750
31	O	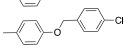	2-methoxy-Ph	8.80	5.056
32	O	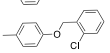	3-OH-Ph	6.08	5.216
33	O			138.60	3.858
34	O		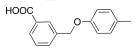	10.12	4.995
35	O		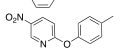	4.61	5.336
*36	O			7.19	5.143
37	O			52.10	4.283

[a] pIC_{50} = -log(IC_{50})
*Indicates external test set compounds
Table 1: Structure and STAT3-DNA inhibitory activities of pyrimidinetriones.

expressing the EGF receptor (NIH3T3/hEGFR) were pre-incubated for 30 min at room temperature with or without increasing concentrations of compound **1** or **2**, prior to incubation with radiolabeled oligonucleotide probe and subjecting to EMSA analysis [23,24]. EMSA results of the binding studies using the hSIE probe show the strongest complex of STAT3:STAT3 with the probe, which was significantly disrupted at 3 μM of compounds **1** and **2** (Figure 1B) and completely disrupted at 10 μM. By contrast, we observe moderate inhibition against STAT1:STAT3 complex formation and insignificant inhibition against STAT1:STAT1 complex formation (Figure 1B). Thus, compounds **1** and **2** preferentially inhibit the DNA binding activity of STAT3 over that of STAT1.

Constitutively activated STAT3 promotes malignant cell proliferation, survival and malignant transformation [5,12,30]. We asked the question whether compounds **1** and **2** will be able to selectively decrease the viability and growth of malignant cells that harbor aberrant STAT3 activity. The human pancreatic (Panc-1) cancer cell line that harbors constitutively active STAT3 and a cell line that does not harbor aberrant STAT3 activity (STAT3 knockout mouse embryonic fibroblasts, MEFs/STAT3-/-) were used as a test case. They were treated with or without increasing concentrations of compound **1** or compound **2** for 72 hours and analyzed for viable cell numbers by CyQuant cell proliferation/viability kit. Compared to the control (DMSO-treated) cells, the malignant pancreatic cancer (Panc-1) cell line showed significantly reduced viable cell numbers following treatment with increasing concentrations of **1** or **2** (Figure 1C). By contrast, the viability of the STAT3-null MEFs (STAT3-/-) cell line, which does not have STAT3 protein, was not significantly altered when treated with the compounds up to 20 μM concentration (Figure 1C). The data together show the specificity/selectivity of the pyrimidinetrione derivatives against STAT3. Therefore, we reasoned that the pyrimidinetrione derivatives could be potentially promising drug leads to modify and develop novel selective STAT3 inhibitors or probe tools for studying STAT3 activity.

Pharmacophore-based 3D-QSAR model

To analyze the quantitative structure-activity relationship (QSAR) of pyrimidinetrione derivatives against STAT3 inhibitory effect, a pharmacophore-based 3D- QSAR modeling approach was adopted (Phase program, Schrödinger, LLC, New York) [31,32]. Thus, we built with a model with a total of 45 commercially available pyrimidinetrione derivatives with diverse structural features (Table 1). The IC_{50} of each compound was tested against STAT3-DNA binding by EMSA analysis as previously described [23,24].

Four topmost active molecules, **1**, **2**, **9** and **10** were chosen to generate a five-feature common pharmacophore hypotheses (CPH) and ranked by survival-inactive score (Sadj) that symbolizes the pharmacophore features present in active molecules but absent in inactive ones. The top ranking CPH (A), AAHRR (A, H bond acceptor; H, hydrophobic; R, aromatic ring) was chosen for aligning the compounds (Figure 2B) and developing an atom-based statistically significant 3D-QSAR model with 35 training set molecules (Table 2). Graphs of observed versus predicted biological activity of the training and test sets used for validation are shown in Figures 2B and 2C. The QSAR model with a high predictive power ($q^2$of 0.604) indicates a good correlation of the biological activity and the independent variables generated from the 3D structures of the compounds.

Additional insights into the influence of structural features on the inhibitory activity could also be gained by visualizing the QSAR model in 3D space. A pictorial view showing the positive or negative influence of particular physicochemical properties is provided in Figure 3. This QSAR

model suggests that the NH group on the barbiturate ring, is a favorable hydrogen bond donor (Figure 3A). The hydrophobic features at R_2 are considered favorable (Figure 3B); furthermore, the model suggests that an electron-withdrawing group on the linker of the two aromatic rings on R_2 group favors inhibitory activity (Figure 3C). Compounds designed were then constructed to match the pharmacophore-based 3D-QSAR model for activity prediction.

PLS Statistic	QSAR Model
Factors	6
r^2	0.9732
q^2	0.604
F	169.3
RMSE	0.3759
Pearson-R	0.797
SD	0.0963

RMSE: Root Mean-Squared Error; SD: Standard Deviation of Regression; r^2: Non-Cross Validated R-squared; q^2: Cross Validated R-squared; F statistic: Overall Significance of the Model; Pearson-R: Pearson Correlation Coefficient

Table 2: PLS statistics of the best QSAR model, obtained with the cis-conformational alignment.

Binding site mapping on STAT3

STAT3 dimerization via reciprocal phosphotyrosine-SH2 interaction between two monomers is considered as a crucial step in STAT3 function. A majority of reported STAT3 inhibitors were designed as STAT3 dimerization disruptors via computational virtual screening on the pY-peptide (APpYLKT) binding "hotspot" on SH2 domain, which consists of the pTyr705 binding pocket (Arg609, Lys591, Glu612 and Ser613), the Leu706 binding subsite and a hydrophobic side pocket (bordered by Ile597, Leu607, Thr622 and Ile634). Other possible inhibitor binding pockets have not been well studied. Thus, we carried out a binding site mapping study using the Sitemap program (Sitemap, Schrödinger, LLC, New York, NY) [33,34], which searched and scored likely binding sites on the STAT3 protein structure (PDB:1BG1 with DNA removed). A DNA binding region on STAT3 DNA binding domain (B) was identified

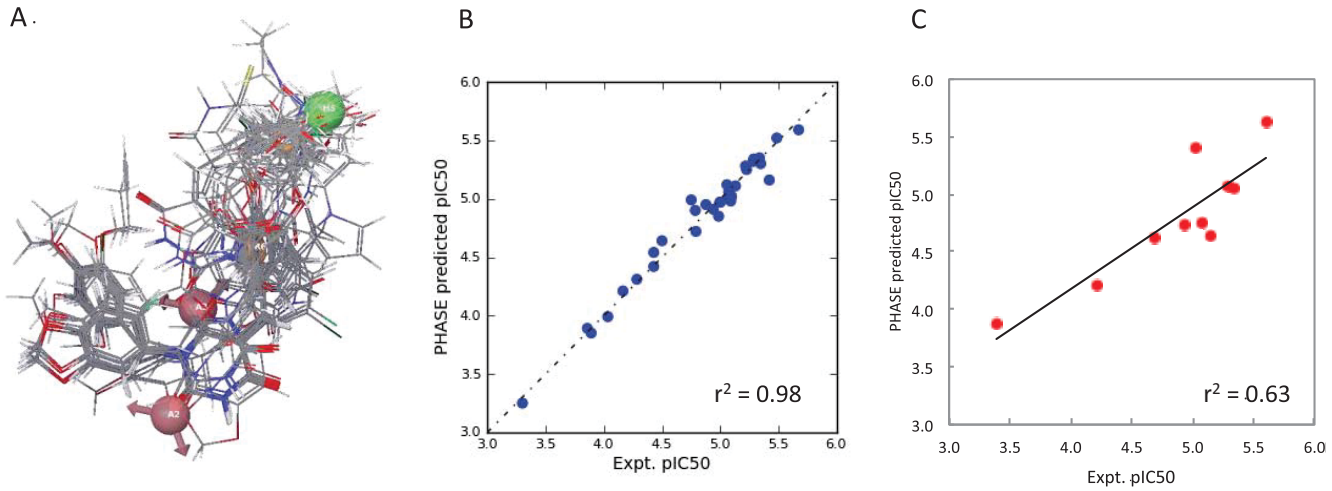

Figure 2: Pharmacophore-based QSAR model with the *cis*-conformation. (A) Alignment of compounds with the 5-point pharmacophore. Plots of QSAR model predicted activity (pIC_{50}) against actual STAT3 inhibitory activities (pIC_{50}) of training set (B) and test set (C) compounds.

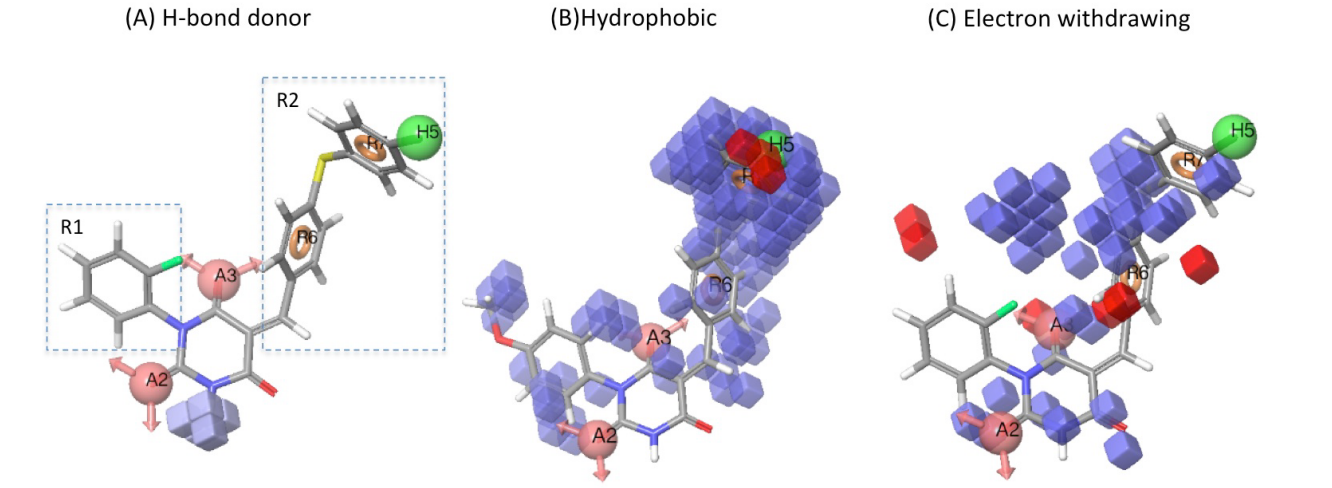

Figure 3: 3D-QSAR model visualized with different features. (A) H-bond donor; (B) Hydrophobicity; and (C) Electron withdrawing property. Light blue cubes surrounding the pharmacophore features represent favorability feature and red cubes represent unfavorability.

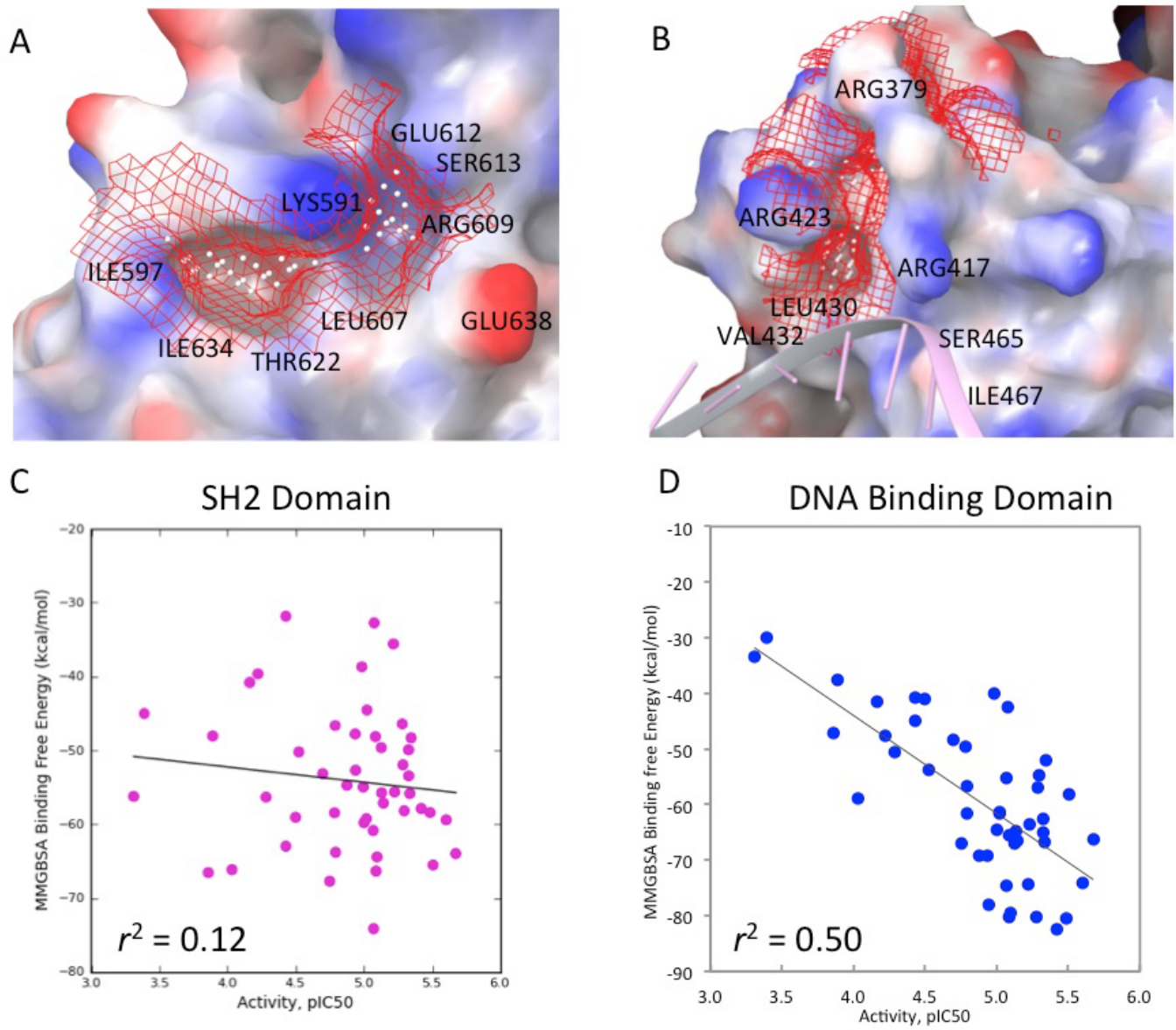

Figure 4: Biding site mapping and MM-GBSA refined docking studies on STAT3. Binding site contour maps of druggable sites on STAT3 (A) SH2 domain and (B) DNA binding domain. White filled circles indicate the size of the site; the red lattice represents the site surface. STAT3 protein surface is represented by electrostatic potential. Red indicates negative charge, and blue indicates positive charge. DNA is represented by the pink helical structure. Plots of STAT3 inhibition activity (pIC_{50}) versus MM- GBSA binding free energy of compounds docked in SH2 domain (C) or the DNA binding domain (D).

as a putative binding site with the highest SiteScore value of 0.990 and the largest cavity (white dots), revealing it as the best druggable site on STAT3. This is interesting information, and could be exploited to advantage, considering that transcription factors are among the most difficult drugagabble targets [28,29]. In contrast, the most commonly targeted SH2 domain (Figure 4A) was assigned a lower SiteScore of 0.662, suggesting that it is an unsuitable druggable site, shallow and narrow. This is a significant observation supporting the recent attention to identifying direct STAT3 DBD binding inhibitors [19] that could change attitudes in attempts at drugging STAT3 [35].

Docking and MM-GBSA rescoring

To examine the binding site of these pyrimidinetriones on STAT3 in light of the above theoretical prediction, we applied docking studies [36,37] of all our tested 45 compounds (Table 1) to both the pY705 binding site and DNA binding site (PDB:1BG1 with DNA removed). Compound poses were then ranked by the Glide GScores. The best-docked compound on STAT3 DNA binding domain and SH2 domain has the GScore value of -5.530 and -4.797, respectively. The highest ranked docking pose of each compound was then subjected to MM-GBSA free energy calculation (Prime, Schrödinger, LLC, New York, NY) which evaluates binding free energies (ΔGbind) by minimization and MD simulation of protein-ligand complexes to address the errors generated by using rigid protein structure in regular docking procedures. Theoretically, potent inhibitors with high affinity ligand-protein binding should generate stable complexes, which have lower

binding energies. In the MM-GBSA rescored binding energy-activity plot, we observed a good correlation (r^2=0.50, with the removal of one outlier) between the MM-GBSA binding free energy and the DNA binding inhibitory activity of the pyrimidinetrione derivatives in the *cis*-isomer configuration at the DNA binding domain (Figure 4D) but not at the SH2 binding domain (Figure 4C). No good correlation was shown with the *trans*-isomer configuration at either site (Suppl. Figure 2). The docking score and binding free energy of Compound **1** in both DNA binding domain and SH2 domain is listed on Suppl. Table 2. These data indicate that the pyrimidinetrione derivatives are likely to bind at the DNA binding domain of STAT3 instead of the supposed SH2 binding hotspot.

The topmost pose of compound **1** (IC_{50}=2.50 μM) with the binding free energy (Δ*G*bind) of -72.591 kcal/mol is shown in Figure 5. The pyrimidinetrione ring of the *cis*-isomer inserted into the cavity and engaged in hydrogen bonding with Leu430 and Val432 (Figure 5A). The inner phenyl ring of the R_2 group participated in π-π interactions with part of Arg423. The chlorine anchored the R_2 group to Asn420. Therefore, the molecule is locked in a fashion that the R_1 phenyl ring pointed toward the binding DNA (DNA structure was brought back into the model after the docking in order to indicate the site), suggesting a preclusion of binding. In addition, the protein structure underwent a large conformational change upon binding of compound **1** (Figure 5C), especially involving loop residues Arg382, Ser465 and Asn466, which interact directly with DNA [38]. This significant conformational change was not observed with the docking of the *trans*-isomers at the same site (Suppl. Figure 3). While R_2 and the pyrimidinetrione core facilitate binding, the R_1 substituent in the *cis*-conformation appears to sterically obstruct the DNA from binding to STAT3. To compare with the recently identified STAT3 DBD binding inhibitor inS3-54A18 [19], we constructed the molecule and docked it to STAT3 DNA binding domain (DBD). The top-ranking pose binds to the domain with a weaker binding free energy (Δ*G*bind) of -59.607 kcal/mol. The Val432 and Gly380 stabilized the carbonyl group and hydroxyl group of inS3-54A18 respectively through hydrogen bonding interactions. The chlorine The chlorine atom anchored the molecule to Asn472 (Figure 5C). Protein conformational change was not observed after inS3-54A18 docking (Suppl. Figure 3B) suggesting that molecule inS3-54A18 might have similar mechanism of inhibition of sterically obstructing the DNA from binding to STAT3; compound **1** has better binding at the STAT3 DBD.

Therefore, a two-step synthesis process described in Scheme 1B was designed to modify the R_1 substituent to increase the steric bulk in order to improve competitive inhibition of DNA binding to STAT3. Compounds with modifications of the R_2 group were also designed to expand the structural diversity keeping drug-likeness in mind (Scheme 1A).

In vitro evidence that designed molecules interact with STAT3 and selectively disrupt STAT3 binding to DNA, but do not disrupt STAT3 binding to cognate pTyr peptide motif

Compounds synthesized were purified and tested for inhibitory activity at the concentration of 10 μM via EMSA analysis. As we expected, compounds **63-67** with bulky and hydrophobic groups at R_1, had the best inhibitory effects against STAT3-DNA binding (Figure 6A). However, the preceding studies do not demonstrate a direct binding, or the binding site on the STAT3 protein. To provide a more definitive evidence of direct binding to STAT3, biophysical studies were performed. Recombinant human GST-tagged STAT3 protein (Abcam, Cambridge, UK) was immobilized on a Biacore CM5 sensor chip for surface plasmon resonance (SPR) analysis of the binding of compounds **63-67** in gradient concentration as analytes. Association and dissociation measurements were made and the binding affinities of the five compounds for STAT3 were determined. The results showed dose-dependent curves of the compounds upon their addition to the immobilized recombinant STAT3 (Figure 6B), indicative of the binding of compound to and dissociation from STAT3 protein. All the compounds exhibited good *K*D values except for compound **63** and **64**, which showed poor solubility in the assay buffer. These data very strong evidence of the direct binding of the pyrimidinetrione STAT3

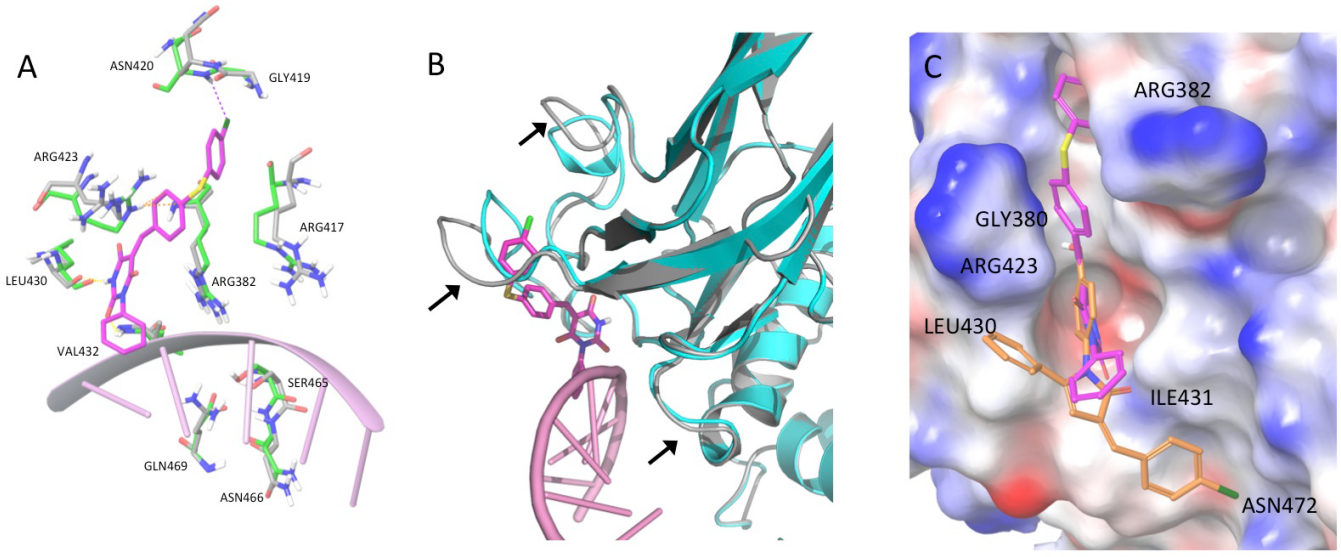

Figure 5: Docking poses of compound 1 and inS3-54A18 at STAT3 DNA binding domain. (*A)* Amino acid shifts induced by compound **1** binding indicated by the green carbon colored amino acid structures. DNA is represented by the pink ribbon and sticks structure. (B) Protein conformational changes shown by overlaying the original structure (gray) and conformation resulting after the MM-GBSA refined docking (cyan). (C) Compound **1** (purple) and inS3-54A18 (orange) docked in STAT3 DNA binding site. Protein surface is presented with electrostatic potential property (red for negative charge and blue for positive charge.

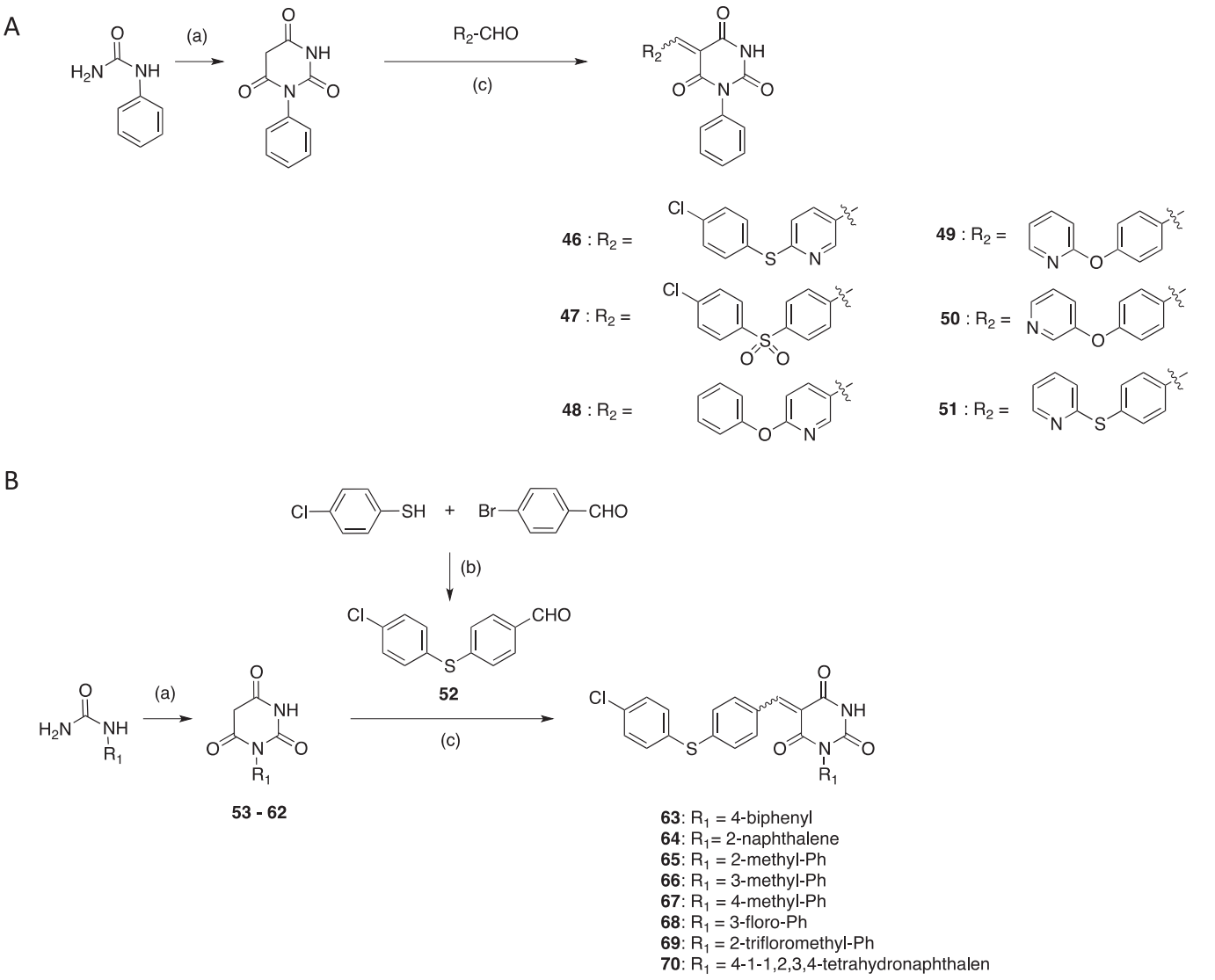

Scheme 1: Synthesis of pyrimidinetrione analogs. Reagents and conditions: (a) Diethylmalonate, NaOEt in 21% ethanol, ethanol, reflux; (b) K2CO3, DMF, 100°C; (c) H_2O, reflux 1 h.

inhibitors to STAT3. These latter studies demonstrate that the designed STAT3 inhibitors **63-67** putatively interact with STAT3 and block STAT3 DNA binding. Given the computational modeling observation that pyrimidinetrione derivatives interact with the STAT3 at DNA binding domain, we surmise that these compounds block STAT3 DNA binding activity by directly disrupting DNA binding, unlike many STAT3 inhibitors that are thought to bind to the SH2 domain. To verify that pyrimidinetrione STAT3 inhibitors directly disrupt STAT3-DNA binding, we chose compound **67** with the best KD value to set up an SPR assay. The 5'-biotinylated hSIE probe was coated on a SA sensor chip. Recombinant STAT3 protein at 0.25 μM with or without **67** (20 μM), as well as **67** (20 μM) alone were incubated for 30 min at room temperature before injecting for SPR analysis as analytes. The data showed that STAT3 protein binds to 5'-biotinylated-hSIE probe with a response unit of 10 and this interaction was dramatically disrupted by adding compound **67** (Figure 7A). Therefore, as we expected from the model, compound **67** inhibits STAT3 binding to DNA by directly binding to STAT3 protein and interferes with DNA binding.

We then extended the studies to verify that **67** does not disrupt the pTyr:STAT3 SH2 domain interaction and subsequently inhibit STAT3:STAT3 dimerization. A similar SPR inhibition assay was designed using biotinylated STAT3-derived pTyr peptide (Biotin-PpYLKTK). The biotinylated STAT3-derived peptide was immobilized on the Biocore SA sensor chip as a ligand; 0.25 μM STAT3 protein with or without 20 μM **67** were incubated at room temperature for 30 min and then subjected to SPR analysis as analytes. No significant interruption of STAT3-pTyr peptide binding was observed in the presence of 20 μM **67** (Figure 7B), which indicated that the binding site of compound **67** on STAT3 was not on the pTyr binding site (SH2 domain) as we predicted in computational studies. This is a very significant result as we can now concentrate our attention on optimizing these new STAT3 inhibitor class using the 3D structures of STAT3 DNA binding domain. This is one of the rare occasions, where computational modeling has been used to elucidate a binding site that has been supported by experimental, direct protein binding studies.

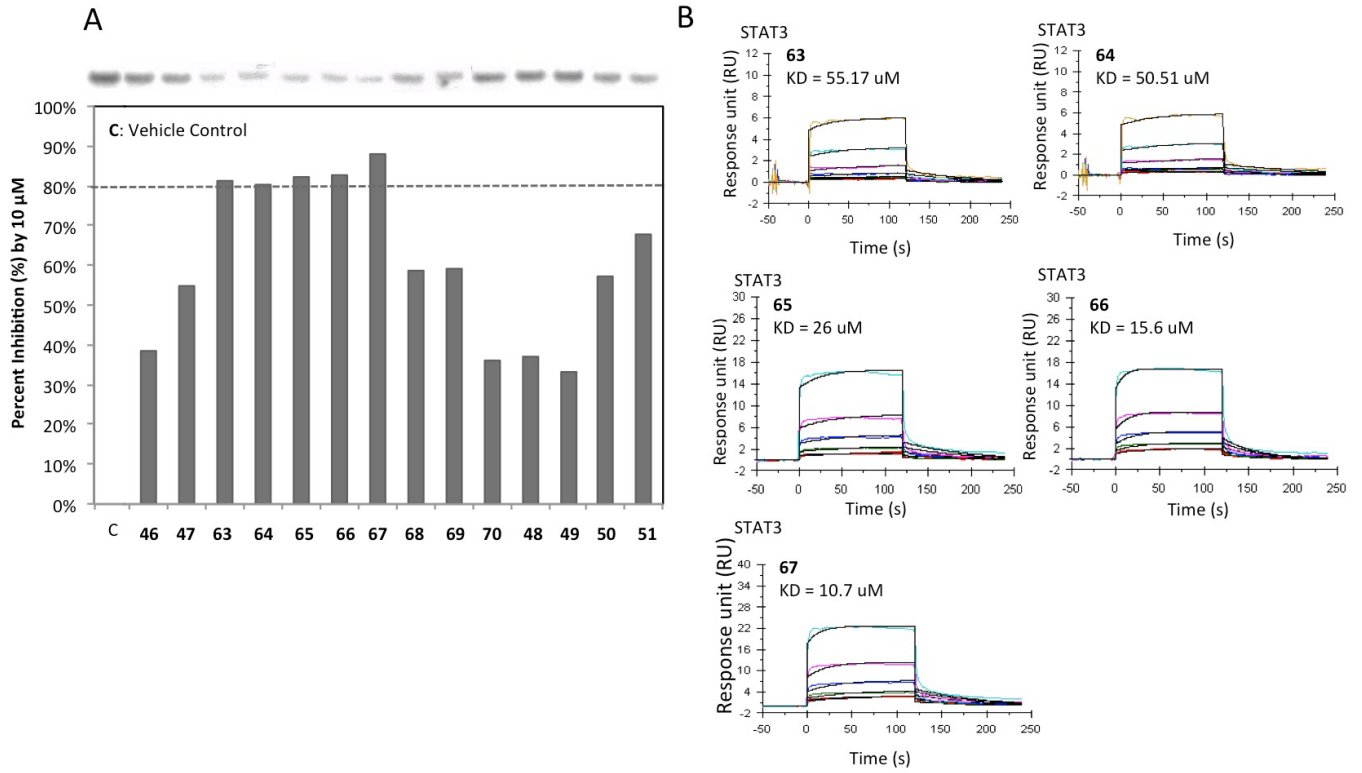

Figure 6: Effects of compounds on STAT3. (A) Percentage inhibition of compounds again STAT3-DNA binding by EMSA analysis. C is the vehicle control. (B) Biacor T200 analysis of compounds **63**-**67** binding of STAT3. STAT3 was immobilized onto a CM5 chip as ligand, and the compounds as the analytes. Compounds were diluted in 1 X PBS (1% DMSO) and filtered. The concentrations are varied from 100 μM to 6.25 μM for compounds **63** and **64**; 50 μM to 3.12 μM for compounds **65-67**.

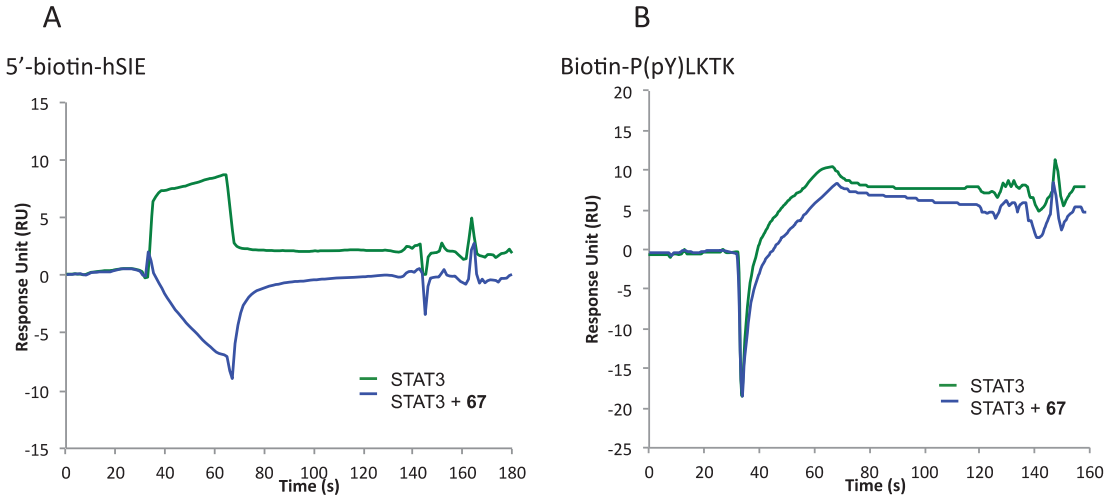

Figure 7: Compound 67 inhibits STAT3-DNA binding (A) but does not interrupt STAT3 dimerization (B). (A) 5'-biotinylated hSIE probe was coated on the SA chip, STAT3 protein (0.25 μm) incubated with or without compound (20 μM) for 30 min prior to the SPR assay. (B) Biotinylated-P(pY)LKTK peptide was coated on the SA chip, STAT3 protein (0.25 μm) incubated with or without compound (20 μM) for 30 min prior to the SPR assay.

Discussion and Conclusion

Although several STAT3 inhibitors have been hypothesized to bind in the STAT3 SH2 domain, the binding sites for small molecule inhibitors of STAT3 have not been identified. STAT3 dimerization via reciprocal phosphotyrosine-SH2 domain interaction between two monomers is considered as a crucial step in STAT3 function. Therefore, inhibiting STAT3 dimerization by displacing the pY-peptide (APpYLKT) binding to its pocket on STAT3 monomer is a rational strategy to inhibit STAT3 function. The binding hot spot on the STAT3 SH2 domain consists of three pockets, pTyr705 binding site (Arg609, Lys591, Glu612 and Ser613), Leu706 binding site and a side pocket (Ile 597, Leu607, Thr622 and Ile634). Using structure-based computational methods including virtual screening and fragment-based drug design, a series of STAT3

dimerization inhibitors, such as STA-21 [39], S3I-201 [40], STX-0119 [41], celecoxib [42] and C188-9 [43], were developed by targeting the STAT3 SH2 domain. However, recent studies have indicated that nuclear import can also take place constitutively and independently of STAT3 tyrosine phosphorylation [20] and the binding of unphosphorylated STAT3 directly to DNA has also been observed [21]. This means that these above mentioned inhibitors could still miss inhibiting STAT3 function and be ineffective against STAT3 driven cancers. Therefore, the traditional strategy of inhibiting STAT3 dimerization may not be an efficient strategy to eliminate functions in tumor cells. Recently, a curcumin-based STAT3 inhibitor HO-3867 was suggested to bind directly to the STAT3 DNA binding domain [44] unlike other STAT3 inhibitors. Meanwhile, only few studies have been accomplished in other STAT3 inhibition strategies or binding site verification, which all the more emphasizes the challenge to STAT3 inhibitor design.

In our study, we discovered a set of novel pyrimidinetrione STAT3 inhibitors with higher inhibitory activity (low micro molar range) than most of the reported STAT3 inhibitors. Interestingly, they selectively inhibit DNA binding to STAT3 over STAT1. In vitro cell viability assays also showed that the compounds tend to inhibit proliferation in cancer cell lines that harbor constitutively active STAT3, relative to STAT3 knock out murine embryonic fibroblast (MEF) cells. This indicates that the pyrimidinetrione STAT3 inhibitors have potential for selective STAT3 targeting. The pharmacophore- based 3D-QSAR model suggested that the substituent at the on R_2 position is critical for STAT3 inhibitory activity. Our structure-based binding site mapping studies suggested the DNA binding domain contains the possible binding pockets for the compounds. From the MMGBSA-refined docking studies, we observed a significant correlation between binding energy at the STAT3-DNA binding domain and STAT3 inhibitory activity when the pyrimidinetrione compounds were docked at the DNA binding site. This energy-activity correlation was not seen with compounds docked to the SH2 domain, suggesting that the pyrimidinetrione STAT3 inhibitors bind at STAT3 DNA binding domain. The docking poses of the most active molecule also suggested that introduction of a hydrophobic or sterically bulky group at R_1 could block DNA binding to STAT3. According to both the QSAR and docking models' observations, new inhibitors were synthesized and tested to confirm their ability to inhibit STAT3. As we predicted, compounds with the 4-((4-chlorophenyl) thio)phenyl substitution at R_2 and bulky group at R1 gained the most inhibitory activity. Biophysics studies provided solid data for compounds directly binding to the STAT3 protein with good *K*D values. We further developed an inhibitory assay using SPR analysis to detect the inhibitory effect of the best synthesized compound, **67**, against STAT3 binding to DNA. Importantly, no significant interruption was observed when compound **67** was used to disrupt the pTyr peptide binding to STAT3. These data together show a strong support of our computational prediction that these novel STAT3 inhibitors disrupted STAT3-DNA binding by directly binding to DNA binding site, unlike many STAT3 inhibitors, which disrupt STAT3 dimerization. In view of the above note that STAT3 dimerization inhibitors may miss the interaction of STAT3 with DNA as even non-phosphorylated STAT3 has been shown to bind DNA and activate transcription. This new class of STAT3 inhibitors may serve as important drug leads or probes for the design and studies of STAT3 DNA-binding site inhibitors that should hold better promise for agent directed at interfering with STAT3 transcription activation.

Experimental Section

Forty-five commercially available pyrimidinetrione derivatives (Table 1) with diverse structural features were chosen by inspection and purchased from ChemBridge (San Diego, CA). Unless otherwise indicated most chemicals and reagents were purchased from Sigma-Aldrich (St. Louis, MI) to follow up on an initial screening of an in-house compound library.

Nuclear extract preparation and electrophoretic mobility shift assay (EMSA). Analyses were carried out as previously described [15,40]. Briefly, the ^{32}P-labeled oligonucleotide probe used was hSIE (high affinity sis- inducible element from the *c-fos* gene, m67 variant, 5'-GCTTCATTTCCCGTAAATCCCTA) that binds STAT1 and STAT3 with high affinity. Nuclear extracts containing activated STAT3 or STAT1 protein were pre-incubated with compound for 30 min at room temperature prior to incubation with the radiolabeled probe for 30 min at 30°C before subjecting to EMSA analysis. Bands corresponding to DNA binding activities were scanned and quantified for each concentration of compound and plotted as percentage of control (vehicle) against concentration of compound, from which the IC_{50} values were derived.

Effects on STAT3 knockout mouse embryonic fibroblasts

Cell lines and reagents: The human pancreatic (Panc-1) cancer cells and the STAT3 null mouse embryonic fibroblasts (MEFs STAT3-/-) have all been previously reported [45]. These cells were grown in DMEM containing 10% heat-inactivated fetal bovine serum (FBS).

Cyquant cell proliferation assay: The CyQuant cell proliferation assay (Invitrogen Corp/Life Technologies Corp) was used to evaluate the biological activities of compounds, as previously reported [45] and following the manufacturer's instructions. Relative cell viability of the treated cells was normalized to the DMSO-treated control cells.

Binding site mapping

The crystal structure of STAT3β homodimer bound to DNA (PDB:1BG1) was imported into Maestro interfaced in the Schrödinger suite. After protein preparation, DNA and water molecules were removed from the structure. Binding site mapping was carried out on the entire protein surface using the SiteMap program (version 2.7, Schrödinger, LLC, New York, NY). The calculation started with placing a 1 Å grid of possible site points around the protein. Grid points in good van der Waals contact with the receptor in solvent-exposed regions enclosed by the receptor served as site points. Then the sites were mapped onto another grid to generate five visualization maps, including hydrophilic, hydrophobic, H-bond donor or acceptor sites. Possible binding pockets were sorted using the SiteScore program, which is constructed and calibrated to 1 with the average score for 157 investigated sites. Therefore, a score greater than 1.0 suggests a very promising site, while a SiteScore below 0.8 indicates a non-drug-binding site [33,34].

Docking

All compounds were constructed in *cis*- and *trans*-conformations and underwent energy minimization and ligand preparation using LigPrep (version 2.8, Schrödinger, LLC, New York), which generated possible ionization states, stereoisomers at pH 7 ± 2. The protein preparation wizard in Maestro was used to prepare the STAT3 protein structure (1BG1) imported from Protein Data Bank (PDB) to render it ready for docking. DNA and water molecules were removed from the structure.

Receptor grid generation and docking studies were carried out with the GLIDE program (version 5.9, Schrödinger, LLC, New York, NY) [36,37]. A receptor grid on the SH2 domain, which can accommodate ligands with length up to 20 Å, was also generated by selecting residues Val637 and Ile 628, located in the center of the SH2 binding pocket, as

the centroid. Similarly, the docking grid at the DNA binding domain was created by picking amino acid residues Val432, Arg382, Glu415, Ser465, Asn466, which were within 3 Å distance from the DNA. Extra-precision (XP) mode of GLIDE docking was executed using a flexible ligand and a rigid receptor routine [46]. Compounds constructed in *cis*- and *trans*-conformations were docked to two binding sites identified by SiteMap. Ten docking poses were obtained from each MM-GBSA Rescoring. Compounds successfully docked were applied to a docking refinement process using the Molecular Mechanics/Poisson-Generalized Born Surface Area (MM-GBSA) implemented in Prime MM-GBSA (version 3.2, Schrödinger, LLC, New York, NY). The analysis, which evaluates binding free energies by minimization and molecular dynamics (MD) simulation of the protein-ligand complex, were utilized to refine the conventional docking scores. The MM-GBSA binding free energy (ΔGbind) between a ligand and its receptor is calculated by the following equation.

$$\Delta G\text{bind}=\Delta H\text{-T}\Delta\text{S}=\Delta E\text{MM}+\Delta G\text{sol}-T\Delta S$$

where ΔEMM is the MM energy difference between the ligand-receptor complex and the sum of the energies of free ligand and unliganded protein, ΔGsol is the corresponding difference in the solvation energies and $-T\Delta S$ is the corresponding difference in conformational entropy upon binding.

Pharmacophore perception

The 45 pyrimidinetrione derivatives and their observed activities expressed as the negative logarithm of measured IC_{50} (pIC_{50}) (Table 1) were used in this analysis. To facilitate the study of isomer influences, each compound was built in *cis*- and *trans*-conformations to generate two different pharmacophore models, respectively. A maximum of 1000 possible conformers (100 conformers per rotatable bond) were generated for each molecule using the MacoModel torsional sampling method (Mixed MCMM/LMOD), followed by 100 steps of minimization using MMFFs force filed in a continuum solvent model. A set of pharmacophore feature sites, including hydrogen bond acceptor (A), hydrogen bond donor (D), hydrophobic group (H), negatively charged group (N), positively charged group (P) and aromatic ring (R), were assigned to each molecule. For both models, activity thresholds of 5.40 and 4.00 were set to identify four actives **2**, **9**, **10** and **28** and four inactive compounds **8**, **14**, **15**, **33**. A pharmacophore with five features common to all the four actives were identified using a tree based partitioning algorithm with a maximum tree depth of five. The pharmacophore box size, which governs the tolerance to match a pharmacophore, was set as 1 Å. The resulting common pharmacophore hypotheses were then ranked by survival score, which represents how well the active compounds superimpose when they are aligned on the features associated with that hypothesis.

Development of 3D-QSAR models

The top ranking common pharmacophore hypotheses was used to align molecules and generate atom-based 3D-QSAR models. The 45 pharmacophore aligned compounds with varying STAT3-DNA binding inhibitory activities were divided as training set and external test set to generate and validate the QSAR model, respectively. The ten test set molecules **2**, **8**, **12**, **16**, **18**, **23**, **36**, **42**, **44** and **45**, were chosen in such a way that they represented the overall biological activity ranges, including the most active molecules, moderately active, and less active molecules. The rest of the molecules, 35 in total, were considered as a training set. The spread of activity (pIC_{50}) in 3D-QSAR models covered approximately 2.4 logs range. In atom-based QSAR, a molecule is treated as a set of overlapping van der Waals spheres. The radii of these van der Walls spheres depend on the atom type in a ligand. Each atom of the ligand is classified into one of the six feature classes, comprising hydrogen bond donor, hydrophobic, negative ionic, positive ionic, electron withdrawing and miscellaneous. A rectangular grid is defined to encompass the space occupied by the aligned ligands. This grid divides the occupied space into consistently sized cubes for dimension of 1 Å, which are occupied by the atoms from the molecule. Therefore, each ligand can be represented by a set of binary-valued (0 or 1) to indicate the occupancy of the cube from different atoms. These occupancies of cubes and atom types are used as independent variables in generation of partial least squares (PLS) regression-based QSAR model [31]. All models were then validated by predicting the activity of the external test set molecules.

Surface plasmon resonance (spr) analysis

Biacore T200 (GE Healthcare, UK) was used for real-time binding interaction studies. For STAT3 and compounds binding analyses, a slow, high-level immobilization of recombinant human GST-tagged STAT3 (ab43618, Abcam, UK) protein was immobilized onto a CM5 series chip (GE Healthcare). The STAT3 protein was diluted to a concentration of 20 ug/mL in 10 mM Acetate buffer (pH=5.0). A 1:1 mixture of N-hyrdoxysuccinimide and N-ethyl-N-(dimethyaminopropyl) carbodiimide was used to activate 2 flow-cells of the CM5 chip. One flow-cell was used as a reference and thus immediately blocked upon activation by 1 M ethanolamine (pH=8.5). The sample flow-cell was injected with the diluted STAT3 at a flow rate of 10 uL/min. The STAT3 injection was stopped when the surface Plasmon resonance reached approximately 8000 RU. The analytes (compounds) were diluted in 1x PBS+1% DMSO buffer (filtered- 0.22 um). The analytes were sequentially injected at a flow rate of 20 uL/min for 120s at 25°C, the dissociation time was set for 2 min. The concentrations were 6.25, 12.5, 25, 50, 100 μM for **63, 64**; 3.125, 6.25, 12.5, 25, 50 μM for **65–67**. The equilibrium dissociation constant (KD) was obtained to evaluate the binding affinity by using the BIAEvaluation 2.0 software (GE Healthcare) supposing a 1:1 binding ratio. At least 3 independent experiments were performed.

For STAT3-DNA inhibition and STAT3-pTyr peptide inhibition assay, the biotin-hSIE probe (5'-biotin-AGCTTCATTTCCCGTAAATCCCTA, ThermoFisher, USA) or biotin-pTyr peptide (biotin-PpYLKTK, Peptide 2.0, Chantilly, VA, USA) was immobilized onto a SA (streptavidin) chip (GE Healthcare). The biotin-hSIE (0.25 μM) or biotin-pTyr peptide (0.25 μM) was diluted in HBS-N and injected at a flow rate of 10 μL/min, The biotin-hSIE injection was stopped when the surface plasmon resonance reached ~724 response difference (RU); the biotin-pTyr peptide injection was stopped at 193 RU. The recombinant human GST-tagged STAT3 (0.25 μM) with or without 20 μM compound 67 were incubated at room temperature for 30 min and then injected over the biotin-hSIE or biotin-pTyr peptide immobilized chip at a flow rate of 25 μL/min for 30 s at 25°C, the dissociation time was set for 1 min. Binding experiments were conducted in 1x PBS+0.2% DMSO as the running buffer, at least 3 independent experiments were performed.

Chemistry

Compounds were visualized by UV light on silica gel coated thin-layer chromatography plates. Flash column chromatography was performed on Fisher silica gel. 1D NMR spectra were recorded on Brucker 300 or 400 MHz NMR spectrometer, using dimethyl sulfoxide (DMSO) as solvent. Melting points of all products were determined using a Fisher-Johns melting apparatus. Mass spectra were obtained on a Brucker-HP Esquire-LC spectrometer (ESI-MS). Analytic high performance liquid chromatography (HPLC) was carried out using a SUPELCOSIL® 5 μm C18 reverse phase column (250 × 4.6 mm) at ambient temperature on a Waters®

2695 HPLC system equipped with the 996 photodiode array detector. An isocratic method comprising 100% methanol (solvent B) was used. Five-min run time was set at a flow-rate of 1.0 mL/min. Area% purity was calculated at 254 nm.

4-((4-Chlorophenyl)thio)benzaldehyde (52)

10 mmol 4-chlorobenzenethiol was dissolved in DMF (5 mL) and equimolar potassium carbonates were added. The resulting reaction mixture was stirred at room temperature for 15 min then 4-bromobenzaldehyde (10 mmol) was added and stirred at room temperature for 4 h. Reaction was monitored using thin layer chromatography. The product was purified by column chromatography. White solid, yield (79 %); M. P. 205-207°C; 1H NMR (400 MHz, DMSO-d6) δ 9.94 (s, 1H), 7.88–7.80 (m, 2H), 7.56 (d, J=0.7 Hz, 4H), 7.38–7.30 (m, 2H); MS (ESI) m/z 270.9 [M+Na]+; HPLC: tR 3.545 min, purity 99.2%.

General procedure for the synthesis of 1-substitued barbituric acids (53-62)

Urea (15 mmol) and diethyl malonate (15 mmol) were added to 250 ml ethanol with NaOEt (15 mmol). The reaction mixture was stirred and refluxed overnight then brought to room temperature. The solvent was partially evaporated and 100 mL cold water was added to the residue, acidified with 1M HCl and placed in ice-bath overnight and the resulting precipitate was filtered off and dried to afford the pure compound.

1-Phenylpyrimidine-2,4,6(1H,3H,5H)-trione (53)

Brown solid, yield 65%; M. P. 261-263°C; 1H NMR (400 MHz, DMSO-d6) δ 11.51 (s, 1H), 7.44 (dq, J=14.3, 7.3 Hz, 3H), 7.24 (d, J=7.5 Hz, 2H), 3.74 (s, 2H). MS (ESI) m/z 202.9 [M–H]-; HPLC: tR 3.001 min, purity 98.0%.

1-([1,1'-Biphenyl]-4-yl)pyrimidine-2,4,6(1H,3H,5H)-trione (54)

White solid, yield 28%; M. P. 220-222°C; 1H NMR (400 MHz, DMSO-d6) δ 11.54 (s, 1H), 7.83–7.65 (m, 4H), 7.51 (dd, J=8.4, 6.9 Hz, 2H), 7.46–7.38 (m, 1H), 7.37–7.28 (m, 2H), 3.76 (s, 2H); MS (ESI) m/z 279.6 [M–H]-; HPLC: tR 2.136 min, purity 99.7%.

1-(Naphthalen-2-yl)pyrimidine-2,4,6(1H,3H,5H)-trione (55)

White solid, yield 18%; M. P. 198-200°C; 1H NMR (400 MHz, DMSO-d6) δ 11.33 (s, 1H), 7.86 (m, 2H), 7.76 (m, 2H), 7.50 (m, 2H), 7.36 (dq, J=7.5, 7.5, 1.5 Hz, 1H), 3.12 (s, 2H); MS (ESI) m/z 252.8 [M–H]-; HPLC: tR 2.677 min, purity 99.3%.

1-(o-Tolyl)pyrimidine-2,4,6(1H,3H,5H)-trione (56)

Yellow solid, yield 39 %; M. P. 225-227°C; 1H NMR (400 MHz, DMSO-d6) δ 11.55 (s, 1H), 7.44–7.23 (m, 3H), 7.18 (d, J=7.6 Hz, 1H), 3.98–3.59 (m, 2H), 2.10 (s, 3H); MS (ESI) m/z 216.9 [M–H]-; HPLC: tR 2.520 min, purity 99.8%.

1-(m-Tolyl)pyrimidine-2,4,6(1H,3H,5H)-trione (57)

White solid, yield 40%; M. P. 210-212°C; 1H NMR (400 MHz, DMSO-d6) δ 11.49 (s, 1H), 7.35 (t, J=7.6 Hz, 1H), 7.23 (dt, J=7.3, 1.3 Hz, 1H), 7.07–6.99 (m, 3H), 3.74 (s, 2H), 2.34 (s, 3H); MS (ESI) m/z 217.0 [M–H]-; HPLC: tR 2.661 min, purity 99.9%.

1-(p-Tolyl)pyrimidine-2,4,6(1H,3H,5H)-trione (58)

White solid, yield 30%; M. P. 238-239°C; 1H NMR (400 MHz, DMSO-d6) δ 11.48 (s, 1H), 7.26 (d, J=8.0 Hz, 2H), 7.11 (d, J=8.0 Hz, 2H), 3.73 (s, 2H), 2.35 (s, 3H); MS (ESI) m/z 217.1 [M–H]-; HPLC: tR 2.529 min, purity 99.7%.

1-(4-Fluorophenyl)pyrimidine-2,4,6(1H,3H,5H)-trione (59)

White solid, yield 29%; M. P. 208-210°C; 1H NMR (400 MHz, DMSO-d6) δ 8.54 (s, 1H), 7.45–7.35 (m, 2H), 7.11–7.00 (m, 2H), 5.83 (s, 2H); MS (ESI) m/z 220.7 [M–H]-, HPLC: tR 2.562 min, purity 97.1%.

1-(3-Fluorophenyl)pyrimidine-2,4,6(1H,3H,5H)-trione (60)

Yellow solid, yield 33%; M. P. 188-189°C; 1H NMR (400 MHz, DMSO-d6) δ 11.61 (d, J=19.0 Hz, 1H), 7.56 (dq, J=15.7, 8.0 Hz, 1H), 7.40–7.25 (m, 1H), 7.17 (p, J=11.6, 10.7 Hz, 2H), 3.78 (d, J=18.4 Hz, 2H); MS (ESI) m/z 221.1 [M–H]-, HPLC: tR 2.629 min, purity 98.4%.

1-(2-(Trifluoromethyl)phenyl)pyrimidine-2,4,6(1H,3H,5H)-trione (61)

White solid, yield 48%; M. P. 174-176°C; 1H NMR (400 MHz, DMSO-d6) δ 11.73 (s, 1H), 7.86 (t, J=9.0 Hz, 2H), 7.69 (s, 1H), 7.56 (d, J=7.9 Hz, 1H), 3.88 (dd, J=166.5, 21.1 Hz, 2H); MS (ESI) m/z 271.1 [M–H]-, HPLC: tR 2.979 min, purity 98.0%.

1-(1,2,3,4-Tetrahydronaphthalen-1-yl)pyrimidine-2,4,6(1H,3H,5H)-trione (62)

Pinkish solid, yield 29%; M. P. 215-217°C; 1H NMR (400 MHz, DMSO-d6) δ 11.29 (s, 1H), 6.92 (m, 4H), 4.95 (d, J=7.0 Hz, 1H), 3.07 (s, 2H), 2.85 (m, 2H), 1.82 (m, 2H), 1.60 (m, 2H); MS (ESI) m/z 256.9 [M–H]-HPLC: tR 1.891 min, purity 98.1%.

General procedure for the synthesis of 5-Benzylidene-pyrimidine-2,4,6(1H,3H,5H)-trione (46-51, 63-70)

1-Substituted barbituric acid (1.0 mmol) was dissolved in boiling water and an appropriate aldehyde (1.0 mmol) was added. The resulting mixture was refluxed with stirring for 1 h. The resulting precipitate was collected by filtration and recrystallized from ethanol to obtain the pure solid.

5-((6-((4-Chlorophenyl)thio)pyridin-3-yl)methylene)-1-phenylpyrimidine-2,4,6(1H,3H,5H)-trione (46)

Yellow solid, yield 65%; M. P. 288-289°C; 1H 1H NMR (400 MHz, DMSO-d6) δ 11.73 (d, J=46.6 Hz, 1H), 8.90 (dd, J=29.6, 2.3 Hz, 1H), 8.44 (ddd, J=33.9, 8.7, 2.3 Hz, 1H), 8.30 (d, J=25.2 Hz, 1H), 7.73–7.66 (m, 1H), 7.66–7.55 (m, 3H), 7.51–7.37 (m, 3H), 7.35–7.27 (m, 2H), 7.12 (dd, J=20.0, 8.6 Hz, 1H); MS (ESI) m/z 433.9 [M–H]-, 465.8 [M-MeOH–H]-; HPLC: tR 1.78 min, purity 99.8%.

1-Phenyl-5-(4-(pyridin-3-yloxy)benzylidene)pyrimidine-2,4,6(1H,3H,5H)-trione (47)

Yellow solid, yield 48%; M. P. 253-255°C; 1H NMR (400 MHz, DMSO-d6) δ 11.68 (d, J=50.7 Hz, 1H), 8.65–8.49 (m, 2H), 8.39 (s, 1H), 8.33 (dd, J=6.6, 2.3 Hz, 1H), 8.28–8.21 (m, 1H), 7.60 (ddd, J=12.9, 8.4, 4.8 Hz, 1H), 7.51–7.44 (m, 3H), 7.28 (d, J=8.2 Hz, 1H), 7.21–7.15 (m, 2H), 7.13–7.00 (m, 2H); MS (ESI) m/z 384.0 [M–H]-, 416.1 [M-MeOH–H]-; HPLC: tR 2.425 min, purity 95.0%.

5-((6-Phenoxypyridin-3-yl)methylene)-1-phenylpyrimidine-2,4,6(1H,3H,5H)-trione (48)

Yellow solid, yield 78%; M. P. 233-234°C; 1H NMR (400 MHz, DMSO-d6) δ 11.73 (d, J=41.3 Hz, 1H), 8.89–8.70 (m, 2H), 8.35 (d, J=25.4 Hz, 1H), 7.54–7.39 (m, 5H), 7.37–7.31 (m, 2H), 7.30–7.26 (m, 1H), 7.26–7.21 (m, 1H), 7.21–7.08 (m, 2H); MS (ESI) m/z 384.0 [M–H]-, 416.0 [M-MeOH–H]-; HPLC: tR 2.291 min, purity 99.73%.

1-Phenyl-5-(4-(pyridin-2-yloxy)benzylidene)pyrimidine-2,4,6(1H,3H,5H)-trione (49)

White solid, yield 50%; M. P. 274-276°C;, 1H NMR (400 MHz, DMSO-d6) δ 11.69 (d, J=63.4 Hz, 1H), 8.36 (d, J=27.1 Hz, 1H), 8.15 (dddd, J=18.6, 4.9, 2.1, 0.8 Hz, 1H), 7.97 (dt, J=39.2, 2.0 Hz, 2H), 7.90–7.80 (m, 2H), 7.57–7.40 (m, 4H), 7.37–7.28 (m, 3H), 7.19–7.13 (m, 1H), 7.08 (ddt, J=21.5, 8.3, 0.8 Hz, 1H); MS (ESI) m/z 384.1 [M–H], 416.1 [M-MeOH–H]-; HPLC: tR 2.121 min, purity 99.0%.

1-Phenyl-5-(4-(pyridin-3-yloxy)benzylidene)pyrimidine-2,4,6(1H,3H,5H)-trione (50)

Yellow solid, yield 48%; M. P. 253-255°C; 1H NMR (400 MHz, DMSO-d6) δ 11.68 (d, J=50.7 Hz, 1H), 8.65–8.49 (m, 2H), 8.39 (s, 1H), 8.33 (dd, J=6.6, 2.3 Hz, 1H), 8.28–8.21 (m, 1H), 7.60 (ddd, J=12.9, 8.4, 4.8 Hz, 1H), 7.51–7.44 (m, 3H), 7.28 (d, J=8.2 Hz, 1H), 7.21–7.15 (m, 2H), 7.13–7.00 (m, 2H); MS (ESI) m/z 384.0 [M–H]-, 416.1 [M-MeOH–H]-; HPLC: tR 2.425 min, purity 95.0%.

7 1-Phenyl-5-(4-(pyridin-2-ylthio)benzylidene)pyrimidine-2,4,6(1H,3H,5H)-trione (51)

Yellow solid, yield 77%; M. P. 266-268°C; 1H NMR (400 MHz, DMSO-d6) δ 11.72 (d, J=55.7 Hz, 1H), 8.54–8.45 (m, 1H), 8.10 (dd, J=25.9, 8.3 Hz, 2H), 7.80–7.71 (m, 1H), 7.65 (td, J=7.7, 1.9Hz, 1H), 7.57 (dd, J=20.6, 8.4 Hz, 3H), 7.27–7.22 (m, 2H), 7.19 (d, J=7.8 Hz, 3H), 6.86 (d, J=8.1 Hz, 1H); MS (ESI) m/z 399.9 [M–H]-, 431.9 [M-MeOH – H]-; HPLC: tR 2.212 min, purity 96.4%.

1-([1,1'-Biphenyl]-4-yl)-5-(4-((4-chlorophenyl)thio) benzylidene)pyrimidine-2,4,6(1H,3H,5H)-trione (63)

Yellow solid, yield 76%; M. P. 272-274°C; 1H NMR (400 MHz, DMSO-d6) δ 11.70 (d, J=56.1 Hz, 1H), 8.30 (d, J=21.4 Hz, 1H), 8.05 (dd, J=29.4, 8.6 Hz, 2H), 7.84 (d, J=8.4 Hz, 1H), 7.78–7.65 (m, 5H), 7.59–7.53 (m, 2H), 7.53–7.47 (m, 2H), 7.45–7.37 (m, 2H), 7.37–7.30 (m, 1H), 7.30–7.23 (m, 1H), 7.23–7.16 (m, 1H); MS (ESI) m/z 509.8 [M–H]-, 540.8 [M-MeOH–H]-; HPLC: tR 1.91 min, purity 98.6%.

5-(4-((4-Chlorophenyl)thio)benzylidene)-1-(naphthalen-2-yl)pyrimidine-2,4,6(1H,3H,5H)-trione (64)

Yellow solid, yield 24%; M. P. 241-243°C; 1H NMR (400 MHz, DMSO-d6) δ 11.80 (d, -1H), 8.31 (d, J=23.7 Hz, 1H), 8.10 (d, J=8.7 Hz, 0H), 8.01 (ddd, J=10.1, 7.3, 3.6 Hz, 2H), 7.94 (t, J=8.6 Hz, 2H), 7.88 (dd, J=5.1, 2.0 Hz, 1H), 7.60 (dt, J=6.6, 3.2 Hz, 1H), 7.58–7.54 (m, 3H), 7.52–7.49 (m, 2H), 7.43 (ddd, J=8.7, 4.9, 2.0 Hz, 1H), 7.25 (d, J=8.6 Hz, 1H), 7.18 (d, J=8.6 Hz, 1H); MS (ESI) m/z 483.8 [M–H]-, 515.0 [M-MeOH–H]-; HPLC: tR 1.96 min, purity 97.8%.

5-(4-((4-Chlorophenyl)thio)benzylidene)-1-(o-tolyl) pyrimidine-2,4,6(1H,3H,5H)-trione (65)

Yellow solid, yield 60%; M. P. 198-199°C; 1H NMR (400 MHz, DMSO-d6) δ 11.72 (d, J=58.8 Hz, 1H), 8.30 (d, J=25.8 Hz, 1H), 8.13–7.97 (m, 2H), 7.56 (d, J=2.0 Hz, 2H), 7.53–7.48 (m,2H), 7.33 (ddt, J=7.9, 4.7, 2.1 Hz, 2H), 7.29–7.15 (m, 4H), 2.08 (d, J=5.3 Hz, 3H); MS (ESI) m/z 449.0 [M–H]-, 478.9 [M-MeOH–H]-; HPLC: tR 2.27 min, purity 99.9%.

5-(4-((4-Chlorophenyl)thio)benzylidene)-1-(m-tolyl) pyrimidine-2,4,6(1H,3H,5H)-trione (66)

Yellow solid, yield 67%; M. P. 214-215°C; 1H NMR (400 MHz, DMSO-d6) δ 11.65 (d, J=56.0 Hz, 1H), 8.27 (d, J=25.5 Hz, 1H), 8.04 (dd, J=29.5, 8.6 Hz, 2H), 7.56 (s, 2H), 7.52 (d, J=3.9 Hz, 2H), 7.34 (d, J=7.9 Hz, 1H), 7.28–7.15 (m, 3H), 7.10 (td, J=2.7, 1.3 Hz, 2H), 2.33 (d, J=6.0 Hz, 3H); MS (ESI) m/z 449.0 [M–H]-, 478.9 [M-MeOH–H]-; HPLC: tR 2.17 min, purity 99.9%.

5-(4-((4-Chlorophenyl)thio)benzylidene)-1-(p-tolyl) pyrimidine-2,4,6(1H,3H,5H)-trione (67)

Yellow solid, yield 67%; M. P. 279-281°C; 1H NMR (400 MHz, DMSO-d6) δ 11.69 (d, J=63.4 Hz, 1H), 8.36 (d, J=27.1 Hz, 1H), 8.15 (dddd, J=18.6, 4.9, 2.1, 0.8 Hz, 1H), 7.97 (dt, J=39.1, 2.0 Hz, 1H), 7.91–7.80 (m, 2H), 7.57–7.39 (m, 4H), 7.37–7.27 (m, 2H), 7.20–7.13 (m, 1H), 7.08 (ddt, J=21.5, 8.3, 0.8 Hz, 1H), 2.10 (s, 3H); MS (ESI) m/z 448.3 [M–H]-, 479.1 [M-MeOH–H]-; HPLC: tR 2.10 min, purity 99.3%.

5-(4-((4-Chlorophenyl)thio)benzylidene)-1-(3-fluorophenyl) pyrimidine-2,4,6(1H,3H,5H)-trione (68)

Yellow solid, yield 71%; M. P. 246-247°C; 1H NMR (400 MHz, DMSO-d6) δ 11.72 (d, J=55.8 Hz, 1H), 8.29 (d, J=26.0 Hz, 1H), 8.11–7.98 (m, 2H), 7.56 (s, 3H), 7.52 (d, J=3.3 Hz, 2H), 7.28 (ddt, J=8.9, 2.5, 1.2 Hz, 1H), 7.26–7.21 (m, 2H), 7.21–7.15 (m, 2H); MS (ESI) m/z 451.9 [M–H]-, 482.9 [M-MeOH–H]-; HPLC: tR 2.27 min, purity 99.9%.

5-(4-((4-Chlorophenyl)thio)benzylidene)-1-(2-(trifluoromethyl) phenyl)pyrimidine-2,4,6(1H,3H,5H)-trione (69)

Yellow solid, yield 46%; M. P. 233–235°C; 1H NMR (400 MHz, DMSO-d6) δ 11.98 (s, 1H), 8.36 (d, J=33.9 Hz, 1H), 8.10 (dd, J=56.0, 8.6 Hz, 2H), 7.92–7.80 (m, 2H), 7.75–7.63 (m, 2H), 7.61–7.50 (m, 4H), 7.31–7.17 (m, 2H), 2.10 (s, 3H); MS (ESI) m/z 501.0 [M–H]-, 533.1 [M-MeOH–H]-; HPLC: tR 1.93 min, purity 99.72%.

5-(4-((4-Chlorophenyl)thio)benzylidene)-1-(1,2,3,4-tetrahydronaphthalen-1-yl)pyrimidine- 2,4,6(1H,3H,5H)-trione (70)

Pinkish solid, yield 26%; M. P. 75-77°C; 1H NMR (400 MHz, DMSO-d6) δ 11.98 (s, 1H), 8.36 (d, J=33.9 Hz, 1H), 8.10 (dd, J=56.0, 8.6 Hz, 2H), 7.92–7.80 (m, 2H), 7.75–7.63 (m, 2H), 7.61–7.50 (m, 4H), 7.31–7.17 (m, 2H), 2.10 (s, 3H); MS (ESI) m/z 489.0 [M–H]-, 519.0 [M-MeOH–H]-; HPLC: tR 3.558 min, purity 82%.

Author Contributions

The manuscript was written through contributions of all authors. All authors have given approval to the final version of the manuscript.

Acknowledgement

We gratefully acknowledge help from Dr. Hemakumar Deokar and financial support from the entities delineated in the Financial Support section below.

Funding Support

Funding from the University of Tennessee Health Science Center (J.K.B, S.S.), as well as Start-up funds from Rosalind Franklin University of Medicine and Science to J.K.B.; National Institutes of Health (NIH)/National Cancer Institute (NCI) Grant CA128865 to J.T.; and the National Institutes of Health Grant S10 RR033072-01 to Y.A-A.

References

1. Darnell JE Jr (2002) Transcription factors as targets for cancer therapy. Nat Rev Cancer 2: 740-749.
2. Stark GR, Kerr IM, Williams BR, Silverman RH, Schreiber RD (1998) How cells respond to interferons. Annu Rev Biochem 67: 227-264.
3. Darnell JE Jr (1998) Studies of IFN-induced transcriptional activation uncovers the Jak-Stat pathway. J Interferon Cytokine Res 18: 549-554.

4. Yu H, Pardoll D, Jove R (2009) STATs in cancer inflammation and immunity: A leading role for STAT3. Nat Rev Cancer 9: 798-809.

5. Yu H, Jove R (2004) The STATs of cancer--new molecular targets come of age. Nat Rev Cancer 4: 97-105.

6. Chapman RS, Lourenco PC, Tonner E, Flint, DJ, Selbert S, et al. (1999) Suppression of epithelial apoptosis and delayed mammary gland involution in mice with a conditional knockout of Stat3. Genes Dev 13: 2604-2616.

7. Darnell JE (2005) Validating Stat3 in cancer therapy. Nat Med 11: 595-596.

8. Costantino L, Barlocco D (2008) STAT 3 as a target for cancer drug discovery. Curr Med Chem 15: 834-843.

9. Chen Z, Han ZC (2008) STAT3: A critical transcription activator in angiogenesis. Med Res Rev 28: 185-200.

10. Kortylewski M, Yu H (2007) Stat3 as a potential target for cancer immunotherapy. J Immunother 30: 131-139.

11. Kortylewski M, Yu H (2008) Role of Stat3 in suppressing anti-tumor immunity. Curr Opin Immunol 20: 228-233.

12. Yue P, Turkson J (2009) Targeting STAT3 in cancer: How successful are we? Expert Opin Investig Drugs 18: 45-56.

13. Schust J, Sperl B, Hollis A, Mayer TU, Berg T (2006) Stattic: A small-molecule inhibitor of STAT3 activation and dimerization. Chem Biol 13: 1235-1242.

14. Song H (2005) A low-molecular-weight compound discovered through virtual database screening inhibits Stat3 function in breast cancer cells. Proc Natl Acad Sci 102: 4700-4705.

15. Siddiquee K, Zhang S, Guida WC, Blaskovich MA, Greedy B, et al. (2007) Selective chemical probe inhibitor of Stat3, identified through structure-based virtual screening, induces antitumor activity. Proc Natl Acad Sci 104: 7391-7396.

16. Lin L, Hutzen B, Li PK, Ball S, Zuo M, et al. (2010) A novel small molecule, LLL12, inhibits STAT3 phosphorylation and activities and exhibits potent growth-suppressive activity in human cancer cells. Neoplasia 12: 39-50.

17. Shahani VM, Yue P, Fletcher S, Sharmeen S, Sukhai MA, et al. (2011) Design, synthesis, and in vitro characterization of novel hybrid peptidomimetic inhibitors of STAT3 protein. Bioorg med chem 19: 1823-1838.

18. Debnath B, Xu S, Neamati N (2012) Small molecule inhibitors of signal transducer and activator of transcription 3 (Stat3) protein. J Med Chem 55: 6645-6668.

19. Huang W, Dong Z, Chen Y, Wang F, Wang CJ, et al. (2015) Small-molecule inhibitors targeting the DNA-binding domain of STAT3 suppresses tumor growth, metastasis and STAT3 target gene expression *in vivo*. Oncogene 35:783-792.

20. Liu L, McBride KM, Reich NC (2005) STAT3 nuclear import is independent of tyrosine phosphorylation and mediated by importin-alpha3. Proc Natl Acad Sci U S A 102: 8150-8155.

21. Nkansah E, Shah R, Collie GW, Parkinson GN, Palmer J, et al. (2013) Observation of unphosphorylated STAT3 core protein binding to target dsDNA by PEMSA and X-ray crystallography. FEBS Lett 587: 833-839.

22. Weidler M, Rether J, Anke T, Erkel G (2000) Inhibition of interleukin-6 signaling by galiellalactone. FEBS Lett 484: 1-6.

23. Turkson J, Zhang S, Mora LB, Burns A, Sebti S, et al. (2005) A novel platinum compound inhibits constitutive Stat3 signaling and induces cell cycle arrest and apoptosis of malignant cells. J Biol Chem 280: 32979-32988.

24. Turkson J, Zhang S, Palmer J, Kay H, Stanko J, et al. (2004) Inhibition of constitutive signal transducer and activator of transcription 3 activation by novel platinum complexes with potent antitumor activity. Mol Cancer Ther 3: 1533-1542.

25. Buerge C, Nagel-Wolfrum K, Kunz C, Wittig I, Butz K, et al. (2003) Sequence-specific peptide aptamers, interacting with the intracellular domain of the epidermal growth factor receptor, interfere with Stat3 activation and inhibit the growth of tumor cells. J Biol Chem 278: 37610-37621.

26. Nagel-Wolfrum K, Buerger C, Wittig I, Butz K, Hoppe-Seyler F (2004) The interaction of specific peptide aptamers with the DNA binding domain and the dimerization domain of the transcription factor Stat3 inhibits transactivation and induces apoptosis in tumor cells. MCR 2: 170-182.

27. Huang W, Dong Z, Wang F, Peng H, Liu JY, et al. (2014) A small molecule compound targeting STAT3 DNA-binding domain inhibits cancer cell proliferation, migration and invasion. ACS Chem Biol 9: 1188-1196.

28. Caboni L, Lloyd DG (2013) Beyond the ligand-binding pocket: targeting alternate sites in nuclear receptors. Med Res Rev 33: 1081-1118.

29. Leung CH, Chan DS, Ma VP, Ma DL (2013) DNA-binding small molecules as inhibitors of transcription factors. Med Res Rev 33: 823-846.

30. Darnell JE (2005) Validating Stat3 in cancer therapy. Nat Med 11: 595-596.

31. Dixon SL, Smondyrev AM, Knoll EH, Rao SN, Shaw DE, et al. (2006) Phase: A new engine for pharmacophore perception, 3D QSAR model development, and 3D database screening:1. Methodology and preliminary results. J Comput Aided Mol Des 20: 647-671.

32. Dixon SL, Smondyrev AM, Rao SN (2006) PHASE: A novel approach to pharmacophore modeling and 3D database searching. Chem Biol Drug Des 67: 370-372.

33. Halgren TA (2009) Identifying and characterizing binding sites and assessing druggability. J Chem Inf Model 49: 377-389.

34. Halgren T (2007) New method for fast and accurate binding-site identification and analysis. Chem Biol Drug Des 69: 146-148.

35. Zhang JT, Liu JY (2016) Drugging the “undruggable” DNA-binding domain of STAT3. Oncotarget 7: 66324-66325.

36. Friesner RA, Banks JL, Murphy RB, Halgren TA, Klicic JJ, et al. (2004) Glide: A new approach for rapid, accurate docking and scoring. 1. Method and assessment of docking accuracy. J Med Chem 47: 1739-1749.

37. Halgren TA, Murphy RB, Friesner RA, Beard HS, Frye LL, et al. (2004) Glide: A new approach for rapid, accurate docking and scoring. Enrichment factors in database screening. J Med Chem 47: 1750-1759.

38. Becker S, Groner B, Müller CW (1998) Three-dimensional structure of the Stat3beta homodimer bound to DNA. Nature 394: 145-151.

39. Song H, Wang R, Wang S. Lin J (2005) A low-molecular-weight compound discovered through virtual database screening inhibits Stat3 function in breast cancer cells. Proc Natl Acad Sci USA 102: 4700-4705.

40. Siddiquee K, Zhang S, Guida WC, Blaskovich MA, Greedy B, et al. (2007) Selective chemical probe inhibitor of Stat3, identified through structure-based virtual screening, induces antitumor activity. Proc Natl Acad Sci USA 104: 7391-7396.

41. Matsuno K, Masuda Y, Uehara Y, Sato H, Muroya A, et al. (2010) Identification of a new series of STAT3 inhibitors by virtual screening. ACS Med Chem Lett 1: 371-375.

42. Li H, Liu A, Zhao Z, Xu Y, Lin J, et al. (2011) Fragment-based drug design and drug repositioning using multiple ligand simultaneous docking (MLSD): Identifying celecoxib and template compounds as novel inhibitors of signal transducer and activator of transcription 3 (STAT3). J Med Chem 54: 5592-5596.

43. Xu X, Kasembeli MM, Jiang X, Tweardy BJ, Tweardy DJ (2009) Chemical probes that competitively and selectively inhibit Stat3 activation. PLoS ONE 4: e4783.

44. Rath KS, Naidu SK, Lata P, Bid HK, Rivera BK, et al. (2014) HO-3867, a safe STAT3 inhibitor, is selectively cytotoxic to ovarian cancer. Cancer Res 74: 2316-2327.

45. Zhang X, Yue P, Page BD, Li T, Zhao W, et al. (2012) Orally bioavailable small-molecule inhibitor of transcription factor Stat3 regresses human breast and lung cancer xenografts. Proc Natl Acad Sci USA 109: 9623-9628.

46. Friesner RA, Murphy RB, Repasky MP, Frye LL, Greenwood JR, et al. (2006) Extra precision glide: Docking and scoring incorporating a model of hydrophobic enclosure for protein-ligand complexes. J Med Chem 49: 6177-6196.